crystals

MDPI

Article

Water-Soluble CdTe/CdS Core/Shell Semiconductor Nanocrystals: How Their Optical Properties Depend on the Synthesis Methods

Brener R. C. Vale, Fernanda O. Silva, Melissa S. Carvalho, Ellen Raphael, Jefferson L. Ferrari and Marco A. Schiavon *

Grupo de Pesquisa em Química de Materiais—(GPQM), Departamento de Ciências Naturais, Universidade Federal de São João del-Rei, Campus Dom Bosco, Praça Dom Helvécio, 74, CEP, São João del-Rei, Minas Gerais 36301-160, Brazil; brenercvale@yahoo.com.br (B.R.C.V.); nandaoliveira_jm@yahoo.com.br (F.O.S.); mel_carvalho_16@hotmail.com (M.S.C.); ellen.raphael@gmail.com (E.R.); jeffersonferrari@gmail.com (J.L.F.)
* Correspondence: schiavon@ufsj.edu.br; Tel. +55-32-3379-2483; Fax: +55-32-3379-2483

Academic Editors: Roberto Comparelli, Lucia Curri and Marinella Striccoli
Received: 31 July 2016; Accepted: 7 October 2016; Published: 15 October 2016

Abstract: We conducted a comparative synthesis of water-soluble CdTe/CdS colloidal nanocrystalline semiconductors of the core/shell type. We prepared the CdS shell using two different methods: a one-pot approach and successive ionic layer adsorption and reaction (SILAR); in both cases, we used 3-mercaptopropionic acid (MPA) as the surface ligand. In the one-pot approach, thiourea was added over the freshly formed CdTe dispersion, and served as the sulfur source. We achieved thicker CdS layers by altering the Cd:S stoichiometric ratio (1:1, 1:2, 1:4, and 1:8). The Cd:S ratios 1:1 and 1:2 furnished the best optical properties; these ratios also made the formation of surface defects less likely. For CdTe/CdS obtained using SILAR, we coated the surface of three differently sized CdTe cores (2.17, 3.10, and 3.45 nm) with one to five CdS layers using successive injections of the Cd^{2+} and S^{2-} ions. The results showed that the core size influenced the optical properties of the materials. The deposition of three to five layers over the surface of smaller CdTe colloidal nanocrystals generated strain effects on the core/shell structure.

Keywords: core/shell; quantum dots; photoluminescence; strain effect; CdTe/CdS

1. Introduction

Various researchers have focused on the synthesis of colloidal nanocrystalline semiconductors, also known as quantum dots (QDs). QDs exhibit intriguing optical properties and find potential technological applications in diodes, electronic devices, lasers, and solar cells [1–4]; they are also applicable as biological markers in the biomedical field [5–9]. From an experimental standpoint, these semiconductors possess unique intrinsic features that stem from the synthetic procedure used to obtain the QDs. Moreover, their optical properties depend on their size and on the possibility to control particle shape and size distribution. Researchers have developed synthetic routes in aqueous medium when they wish to achieve QDs. These routes are easily reproducible, inexpensive, and less toxic than the organic synthesis route; moreover, they afford water-soluble and thus biocompatible nanoparticles [10–13].

All of these advantages have prompted research into water-soluble QDs, aiming to increase the photoluminescence quantum yield (QY) of the materials synthesized in aqueous medium [4]. In this context, an important strategy is to prepare structures of the core/shell type. Besides enhancing the photoluminescence QY, these systems improve nanocrystals' photostability. In addition, an appropriate choice of the components of the core and shell might extend the emission of the resulting materials over a wide range of visible spectrum wavelengths [14].

Nanocrystalline semiconductors of the core/shell type result from the combination of at least two distinct semiconductors: one of them constitutes the core; the other constitutes the shell—an external layer that coats the core. The advances in new synthesis techniques make it possible to synthesize not only symmetrical (spherical) nanoparticles, but also a variety of other shapes, such as cubes, disks, wires, rods, and tubes [15]. Depending on the energy bands' separation, semiconductor/semiconductor core/shell nanoparticles can also be classified into three different groups: type I, reverse type I, or type II. In the first case, the energy band gap of the shell material is wider than the band gap of the core material. The electrons and holes are confined within the core because both the conduction-band and the valence-band edges of the core are located within the energy gap of the shell [16]. These types of semiconductor particles can be made from CdSe/CdS, CdSe/ZnS, or CdTe/CdS. Reverse type I is the reverse case of that presented before. In this case, both hole and electron charges are partially delocalized on the shell materials and the emission wavelength can be tuned by changes in the thickness of the shell. The most extensively studied systems in this category are CdS/CdSe and ZnS/CdSe. Type II core/shell systems, in contrast to type I, have both the valence and conduction band of the core either lower or higher than those in the shell. As a result, one carrier is mostly confined to the core, while the other is mostly confined to the shell. Therefore, the energy gradient existing at the interfaces tends to separate the electrons and holes spatially on different sides of the heterojunction [16,17]. Some common examples of this type of core/shell are CdTe/CdSe, CdSe/ZnSe, PbSe/CdSe, PbSe/CdSe, and CdS/ZnSe.

One important feature of semiconductor/semiconductor core/shell nanocrystals is the influence that the shell plays on their optical properties. Besides the compositions of the semiconductors, the variation of the shell thickness can also have an important role in changing the optical properties of core/shell QDs [18]. It has already been demonstrated that the absorption and emission peak positions of CdTe and CdS-coated CdTe are shifted to a higher wavelength with increasing reaction time, with increase in the QY [19]. Klimov et al. [20] demonstrated that the core-to-shell transition could be tuned by simply controlling the shell thickness. They prepared ZnSe/CdSe, which is a reverse type I core/shell nanoparticle, so that with increasing shell thickness the transition from type I to type II and back to type I can occur.

Because core/shell systems comprise two distinct semiconducting materials, they are also subject to strain effects that may alter the nanocrystals' optical and electronic properties or even change the behavior of type I core/shell structures into type II behavior [18]. It was pointed out that the strain induced by the lattice mismatch could be used to tune the light emission of lattice-mismatched core/shell QDs. In solar cell devices, core/shell structures serve as a strategy to enhance photovoltaic cell yields because they promote efficient charge separation. While core/shell structures of type I can create a barrier to electron transfer, in type II, for example, the shell might function as a bridge, favoring electron transfer [21–23].

Regarding the experimental synthetic routes to prepare core/shell QDs, one- or two-step experimental procedures generally afford such kinds of structures. Nevertheless, it is always desirable to simplify experimental methods and obtain water-soluble QDs with improved properties. The two-step synthesis involves initial production of the core nanocrystals, followed by nanocrystals' purification via precipitation, nanocrystals' dispersion in an appropriate solvent, and subsequent growth of the shell constituent around the core material. This procedure is advantageous: one can eliminate impurities and reaction products generated during the first step. As for the one-step approach, the purification step does not exist, and the shell material has to be directly grown on the freshly prepared core [24]. Peng et al. [25] were the first to propose the SILAR (successive ionic layers and adsorption reaction) technique to obtain core/shell systems, which consists of a two-step strategy. These authors grew a CdS shell around a colloidal CdSe core prepared in organic medium.

To grow an external layer efficiently over the core region, it is important to take the lattice mismatch of the core and shell materials into account. The larger the mismatch in the lattice parameter between the core and the shell, the greater the effect of stress on the core. Moreover, this parameter

must be small, to facilitate crystallization and growth of both constituents in the same structure. In addition, to prevent defects from appearing on the surface of the core/shell interface, it is necessary that the shell material display high reactivity and selectivity toward the core material. It is also crucial to control shell thickness efficiently; a thin shell is not sufficient to correct surface defects, while a thick shell may cause the transformation of core/shell type I to type II or vice versa, due to the compression effect on the core [26,27]. Smith et al. [18] reported that a thicker shell elicited CdTe/ZnSe conversion from a type I to a type II system because the strain over the core constituent increased.

Although the concept of strain-induced defect formation has been the predominant criterion for understanding the photoluminescence features of core/shell QDs, the relationship between lattice mismatch of the semiconductors and the photoluminescence efficiency of core/shell QDs remains controversial in the literature. While for ZnTe/CdSe type II core/shell with only 0.6% of lattice mismatch the QY was between 15% and 20%, for the CdTe/CdSe and CdTe/ZnS type II core/shell with 7.1% and 19.8% lattice mismatch the QYs were about 50% and 60%, respectively [18].

In this study, we synthesized CdTe/CdS type I core/shell systems via colloidal chemistry in aqueous medium using two different routes: the one-pot approach and two-step synthesis (SILAR). The latter route allows one to increase the CdS shell thickness from one to five layers of growth on CdTe cores of different sizes to obtain information about strain effects and their influence on the optical properties. To simplify the synthesis method, we have employed the one-pot approach by using a CdTe core and batch growth of the CdS shells. The optical properties were studied and a proper comparison between both materials was performed.

2. Results

In both experimental methods investigated here, we obtained the CdTe core by adding the precursor NaHTe to the solution containing the surface ligand 3-mercaptopropionic acid (MPA) and Cd^{2+} ions [28]. Figure 1 displays the UV–vis absorption and photoluminescence (PL) spectra relative to the time evolution of the CdTe core during the synthesis. The absorption and emission bands shifted to longer wavelength—from 471 to 522 nm (Figure 1a) and from 514 to 557 nm (Figure 1b), respectively—demonstrating that nanoparticle size increased as the procedure progressed. The absorption spectra are assigned to the well-defined first excitonic $1S_{3/2}(h) \rightarrow 1S(e)$ transition. The inset in Figure 1a shows a typical image of the CdTe core obtained with 4 h of synthesis, and reveals virtually spherical and well-dispersed nanocrystals; no aggregation occurred after the surface ligand MPA was replaced by 1-dodecanethiol (DDT). The procedure for ligand exchange and the histogram of the particle size distribution is in the Supplementary Material. The calculated size from the empirical equation proposed by Peng et al. [29] gave a size of 2.8 nm, which is in agreement with the histogram obtained from TEM analysis (Figure S1).

We used different CdTe core sizes (2.17, 3.10, and 3.45 nm) for the SILAR method. For the one-pot approach, we employed the CdTe core achieved at 10 min of reaction, with particles of 2.10 nm.

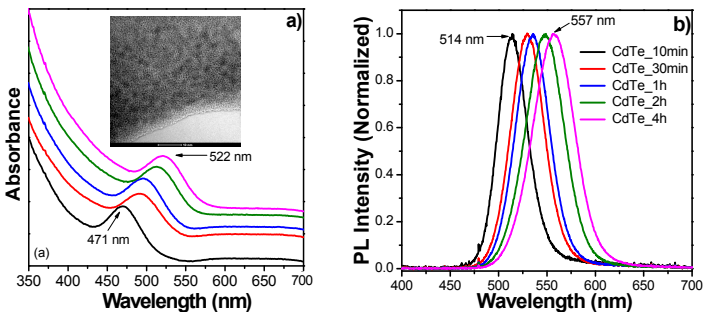

Figure 1. UV–vis absorption (**a**) and photoluminescence (PL) (**b**) spectra of the CdTe nanocrystals stabilized with the ligand 3-mercaptopropionic acid (MPA). Inset in (**a**): TEM image of the CdTe nanocrystals, obtained with 4 h of synthesis, containing 1-dodecanethiol (DDT) as surface ligand.

2.1. CdTe/CdS QDs Synthesized via the SILAR Method

Core/shell QDs were synthesized according to previous methods reported in the literature with a few modifications [25,30]. To determine the amount of Cd^{2+} and S^{2-} precursors necessary to grow each CdS monolayer, we used a literature method [25,29,30]. For experimental details, see in Table S1 in the Supplementary Material.

Figure 2 displays the UV–vis and the PL spectra of the CdTe/CdS QDs prepared with one to five layers of CdS and CdTe core of 2.17 nm diameter. The absorption and emission bands shifted to longer wavelength as the number of CdS layers deposited around the CdTe nanocrystals increased. This shift is attributed to a reduced quantization of the electron due to increase in the size of the nanoparticle, and the spreading of the respective wave functions into the CdS shell [31]. In the particular case of the emission spectra, the band shifted from 537 nm in the CdTe nanocrystals spectrum to 671 nm after deposition of five CdS layers (variation of ~134 nm). This large shift of the emission band suggests the formation of a core/shell structure rather than an alloy. Figure 2c clearly shows that the CdTe nanocrystals coated with two to three CdS layers exhibited more intense luminescence. Growing more than three CdS layers around the CdTe nanocrystals reduced both absorption (Figure 2a) and emission (Figure 2c) band intensities. This could be ascribed to transformation of the CdTe/CdS core/shell system from type I to type II [18]. In this case, deposition of three to five layers of the shell constituent over the surface of the nanocrystals' core may have given rise to strain effects, which may have separated the charge carriers: the holes and electrons remained on the core and shell regions, respectively. The deposition of one to three layers probably conferred on the QDs a behavior that was intermediate to those of type I and II systems, a situation known as "*quasi* type II". In this state, the holes remain in the core region, while the electrons are delocalized on the core/shell interface, which does not significantly alter the nanocrystals' absorption or emission bands. Nevertheless, demonstrating conversion of type I core/shell systems into type II systems still involves an increase in the excited state lifetime. We did not evaluate this parameter, so the attenuated absorption and emission band intensities suggest this transformation is due to a gradual reduction of distinct optical absorption features and a decrease in the band-edge oscillator strength. These changes are caused by spatial separation of holes into the core and electrons into the shell, resulting in a decrease in the electron–hole overlap integral [18,26].

The cause of the transformation of core/shell type I into type II is due to two factors that are related to each other: increasing the thickness of the CdS shell and compression of the shell onto the core. The increased thickness of the CdS shell causes an increase of the energy level of the valence band, whereas the conduction band decreases with the materials tending to behave like bulk. At the same time, with increasing shell thickness is generated a core compression effect due to the mismatching of the lattice parameters between the core and shell, and the result is that the energy level of the core conduction band shifts to lower energy [32]. Thus, the alignment of the band energy levels of the valence and conducting bands of the core and shell, which initially fell within a type I system, shall fall in a type II system. Scheme 1 shows a representation of this effect.

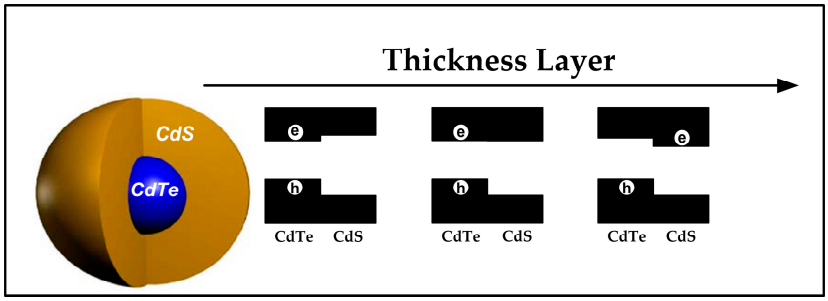

Scheme 1. Scheme of the change of the energy levels due to the increased thickness of the shell.

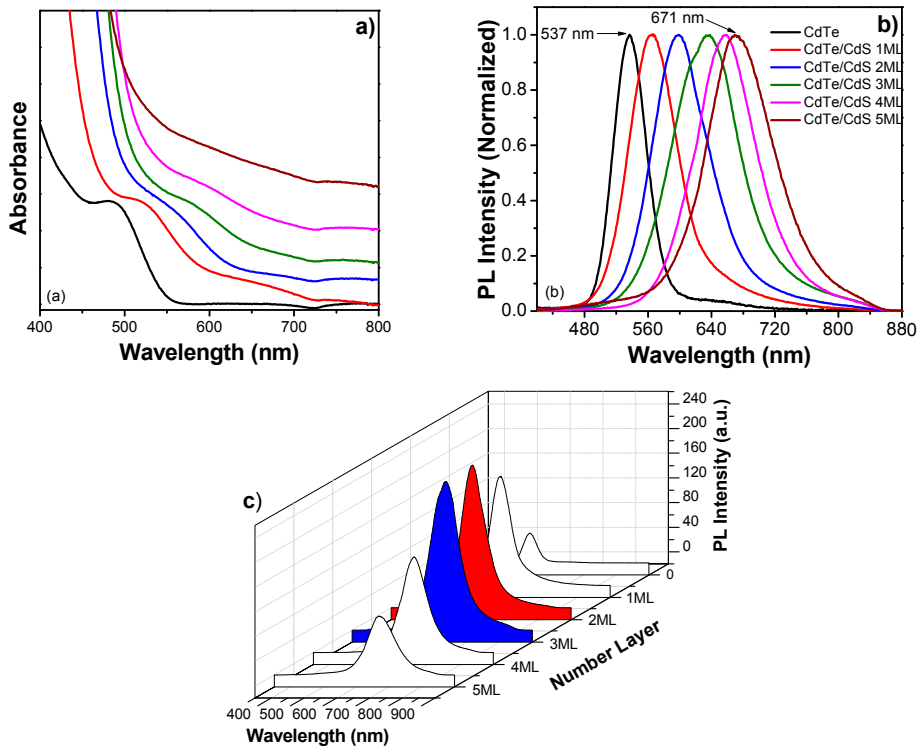

Figure 2. UV–vis absorption (**a**) and PL spectra (**b**) and (**c**) of CdTe/CdS QDs with one to five layers of CdS synthesized with CdTe core of 2.17 nm diameter.

Figure 3 illustrates the X-ray diffractograms of the CdTe/CdS core/shell systems synthesized with CdTe nanocrystals of 2.17 nm. The QDs presented diffraction peaks at approximately 24.5°, 40.5° and 48.0° (2θ), corresponding to the planes (111), (220), and (311), respectively, which refer to crystalline structure of the zinc blende type (JCPDS 65.1046) [33]. In addition, we detected considerable displacement of the diffraction peaks toward CdS as the number of CdS layers deposited on the CdTe nanocrystals increased. Moreover, a larger number of CdS layers improved the crystallinity of the material because CdS grew layer by layer (ICDD No. 75-1546).

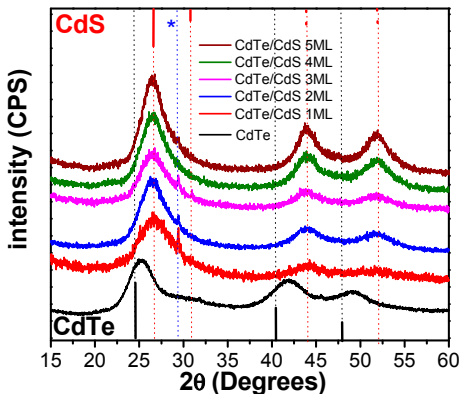

Figure 3. X-ray diffraction patterns of CdTe core and CdTe/CdS core/shell quantum dots (QDs) with different numbers of layers (one to five) of CdS. * Impurities or byproducts not identified in the JCPDS data base.

To investigate how core size and monolayer thickness affected the QDs' optical properties, we also prepared CdTe/CdS core/shell systems using CdTe nanocrystals with diameters of 3.10 and 3.45 nm;

we then coated these nanocrystals with one to five CdS layers. Table S2 (Supplementary Material) lists the molar quantities of the Cd and S precursors that were necessary to grow these layers around the CdTe nanocrystals of 3.10 nm.

Figure S2 shows the UV–vis and PL spectra of CdTe/CdS QDs prepared with CdTe nanocrystals of 3.10 nm. The absorption and emission bands shifted from 538 to 606 nm and from 571 to 662 nm, respectively, as the number of CdS layers deposited over the CdTe nanocrystals increased, similar to the observation for CdTe nanocrystals of 2.17 nm. More specifically, the emission band shifted by ~91 nm, but this value was smaller than the shift found for the CdTe/CdS QDs prepared with CdTe nanocrystals of 2.17 nm (~134 nm). Figure S2 revealed that the CdTe nanocrystals of 3.10 nm with three CdS layers displayed the most intense luminescence. Deposition of three to five CdS layers did not diminish the emission (Figure S2c) or the absorption (Figure S2a) intensity as significantly as in the case of CdTe/CdS QDs prepared with CdTe nanocrystals of 2.17 nm.

Table S3 contains the Cd and S precursors' molar quantities that were required to grow between one and five CdS layers around the CdTe nanocrystals of 3.45 nm. Figure S3 illustrates the UV–vis and the PL spectra of these QDs at 6 h of synthesis. Once again, the absorption and emission bands shifted toward longer wavelengths, attesting that a higher number of CdS layers on the CdTe nanocrystals provided larger QDs. We verified absorption and emission band shifts of ~50 and ~70 nm, respectively. Like CdTe nanocrystals of 3.10 nm, CdTe nanocrystals of 3.45 nm containing three CdS layers displayed maximum luminescence intensity. Figure S3a,c also demonstrate that the absorption and emission intensities did not significantly decrease for four and five deposited CdS layers.

Figure 4a revealed that the emission bands' position varied as a function of the number of CdS layers deposited on the CdTe/CdS QDs synthesized with CdTe nanocrystals of 2.17 nm, 3.10 nm, and 3.45 nm as follows: ~134, ~91, and ~70 nm, respectively. Three explanations exist for this trend: (1) Smaller nanocrystals afforded larger displacement because they were more susceptible to the strain effects that the CdS layers exerted over the core surface. These effects may have extended the luminescence spectra of these materials from the green to the near infrared regions [18]; (2) Thicker layers did not effectively compress the cores consisting of slightly larger nanocrystals (CdTe nanocrystals of 3.10 nm and CdTe of 3.45 nm), so their emission bands shifted significantly less; (3) Thicker CdS layers may have grown on smaller nanocrystals (CdTe nanocrystals of 2.17 nm, Table S2), which may have favored strain effects as compared with the CdS layers grown on larger nanocrystals.

We determined the fluorescence QYs for the CdTe/CdS QDs prepared with different core sizes and shell thicknesses using the comparative method of Williams et al. [34]. Relationship between absorbance and integrated fluorescence intensity for rhodamine 101 (standard) and CdTe/CdS QDs with three CdS layers are shown in Figure S4. The values of the fluorescence QYs of the CdTe and CdTe/CdS core/shell are shown in Figure 4b. The CdTe/CdS QDs prepared with CdTe nanocrystals of 3.10 nm furnished the largest QY: 81%. We also verified that the QDs prepared with CdTe nanocrystals of 3.10 nm and CdTe nanocrystals of 3.45 nm presented maximum QY when they contained three CdS layers, whereas the QDs prepared with CdTe nanocrystals of 2.17 nm achieved maximum QY with one CdS monolayer. This result was quite similar to that shown in Figure 1c, Figures S1c and S2c. In all cases, QY diminished with increasing number of CdS layers on the CdTe nanocrystals, as a result of strain effects. Combined with the high surface reactivity of the nanocrystals, these effects may have generated CdTe surface defects on the nanocrystals, lowering the QY values. This reduction was more noticeable for the CdTe/CdS QDs prepared with CdTe nanocrystals of 2.17 nm because strain usually affects smaller nanocrystals more significantly. This phenomenon probably elicited transformation of core/shell type I systems into type II systems. Hence, the electron wave function is restricted to the shell, and the quality of the nanocrystals' surface plays a more essential role in fluorescence QY. Because they were more susceptible to compression, CdTe nanocrystals of 2.17 nm probably contained more surface defects, which determined an abrupt decrease in QY when more than one CdS monolayer was deposited on the core [35].

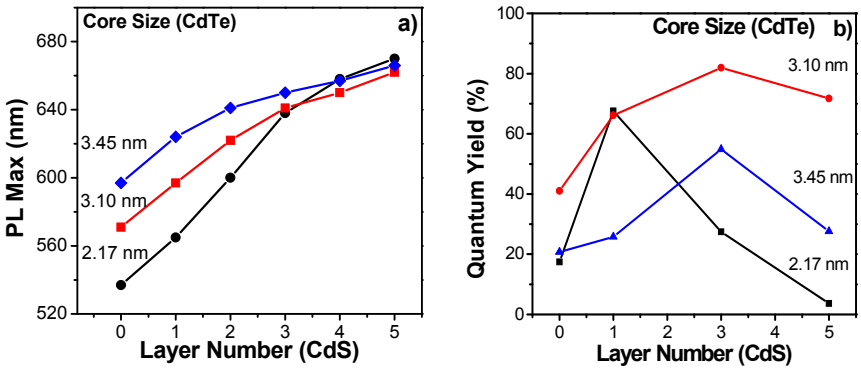

Figure 4. (**a**) Variation in the emission band positions and (**b**) fluorescence quantum yield values for the CdTe/CdS QDs obtained with CdTe nanocrystals of 2.17 nm, 3.10 nm, and 3.45 nm.

Figure 5 corresponds to the plots of the full width at half maximum (FWHM) as a function of the number of CdS layers for the CdTe/CdS QDs prepared with CdTe nanocrystals of different sizes. All of the plots revealed that the FWHM values increased as more CdS layers grew on the nanocrystals' surface. In other words, CdS deposition elicited a larger size distribution of QDs [17], probably because CdS did not homogeneously coat the CdTe core. Figure 5 demonstrates that the CdTe nanocrystals of 2.17 nm exhibited a wider size distribution for a larger number of deposited CdS layers. This happened because smaller nanocrystals were more susceptible to strain effects, which may have prompted size polydispersion. It is important to emphasize that some core/shell systems like CdSe/CdS present FWHM values that do not depend on the shell's constituent thickness. This suggests good control of nanocrystals' size distribution as larger amounts of the shell constituent grow on the shell [25].

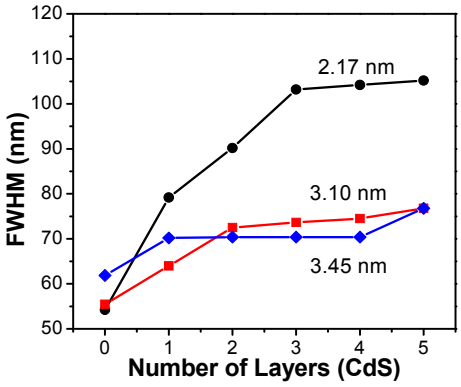

Figure 5. Full width at half maximum (FWHM) values for CdTe/CdS QDs prepared with CdTe nanocrystals of 2.17 nm, 3.10 nm, and 3.45 nm.

2.2. CdTe/CdS QDs Synthesis via the One-Pot Approach

For the one-pot approach, we used thiourea as the sulfur ions precursor. The excess Cd^{2+} ions from the synthesis of the CdTe core reacted with the S^{2-} ions released from thiourea to form CdS; the latter was arranged around CdTe to furnish the CdTe/CdS structure [32,36]. The deposition of a thin CdS monolayer over these CdTe nanocrystals can generate CdTe/CdS core/shell with a 1:1 Cd:S ratio. Figure 6 presents the UV–vis and PL spectra obtained as the synthesis of these systems evolved.

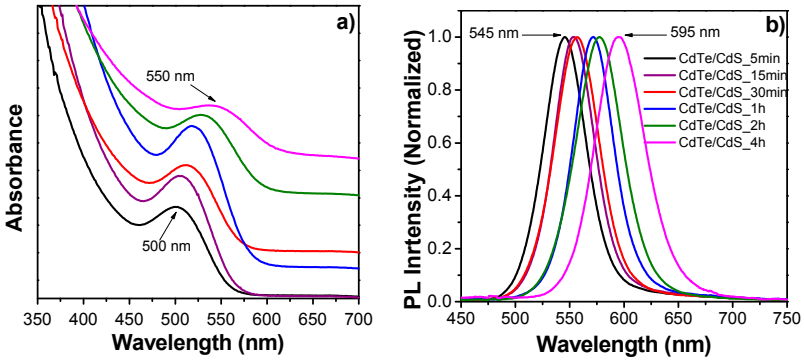

Figure 6. (**a**) UV–vis absorption; (**b**) PL spectra of the CdTe/CdS 1:1 core/shell growth with a Cd^{2+}:thiourea (S^{2-}) molar ratio of 1:1.

The absorption and emission bands also shifted toward longer wavelength during the synthesis of the CdTe/CdS system—from 500 to 550 nm (Figure 6a) and from 545 to 595 nm (Figure 6b), respectively—revealing that the QDs' size increased during the process. A comparative analysis of these UV–vis and PL spectra with those of CdTe nanocrystals (Figure 1) showed that the CdTe/CdS 1:1 system and the CdTe nanocrystals bearing MPA as surface ligand exhibited similar shifts toward longer wavelength. In the case of the CdTe nanocrystals (Figure 1), ~51- and ~43-nm shifts occurred for the absorption and emission bands, respectively; for the CdTe/CdS 1:1 system, both absorption and emission bands shifted by ~50 nm (Figure 6). The CdTe/CdS 1:1 core/shell contains only a thin CdS layer around CdTe, so these similarities demonstrated that no significant changes in the optical properties of the CdTe core occurred upon CdS deposition.

Figure 7 illustrates the UV–vis absorption and PL spectra of the CdTe/MPA nanocrystals and the CdTe/CdS 1:1, 1:2, 1:4, and 1:8 core/shell systems recorded at 3 h of synthesis.

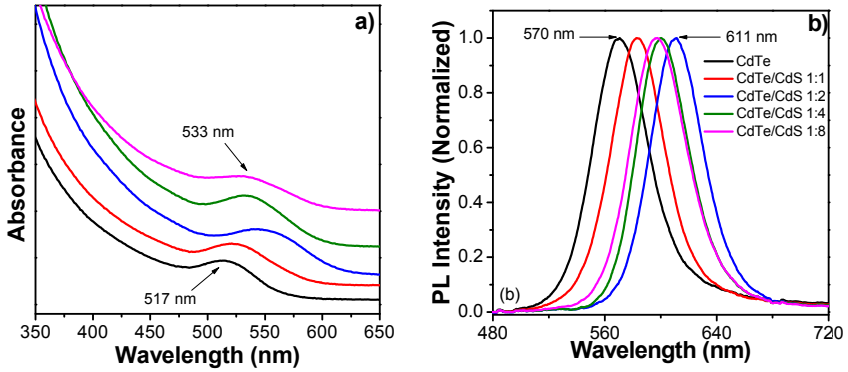

Figure 7. (**a**) UV–vis absorption, (**b**) PL spectra of the CdTe/MPA nanocrystals and the CdTe/CdS core/shell growth with Cd^{2+}:thiourea (S^{2-}) molar ratios of 1:1, 1:2, 1:4, and 1:8.

For both UV–vis and PL spectra, the bands shifted toward longer wavelengths in the case of the CdTe nanocrystals and the CdTe/CdS 1:1 and 1:2 core/shell systems because of weakening of the quantum confinement effect, which is due to the increase of the particle size and the formation of the CdS shell. As for the CdTe/CdS 1:4 and 1:8 core/shell systems, the absorption and emission bands display a blue shift, which may be due to the synthesis method used and the precursor source. In this method, the sulfide precursor is added all at one time; in contrast, the SILAR method grows layer by layer with successive additions of the precursor. The source of sulfide in the one-pot method is a molecular compound that has to be degraded, and thus the release of sulfide ions is slow, which is also in contrast to the SILAR method, which uses sodium sulfide as a precursor and reacts instantly.

Thus, at higher concentrations of thiourea, this molecule can cause steric hindrance and prevent the sulfide ions diffusing to the surface of the QDs, slowing the growth of the material.

Figure 8 shows the QY results of CdTe/CdS QDs obtained using the one-pot method. It was observed that with the addition of thiourea there was a considerable increase in the QY, indicating passivation of the surface and consequent decreasing of surface defects. With increasing ratio of thiourea and Cd^{2+} the QY tended to increase and reached a maximum at a ratio of 4:1. In the ratio of 8:1 there was a small decrease but QY still remained high at ~40%. It is noteworthy that the core CdTe employed was the one with only 10 minutes of synthesis, with average size 2.1 nm, and still has not seen a dramatic decrease in QY, demonstrating that there was no growth of a thick layer of CdS on the core CdTe. As noted above, such growth causes compression of the CdTe core and leads to changing the core/shell from type I to type II.

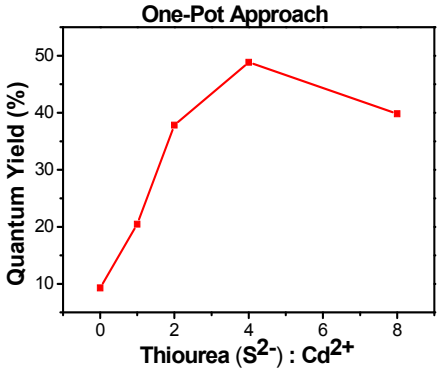

Figure 8. Fluorescence quantum yield (QY) versus ratio thiourea/Cd^{2+} via the one-pot approach.

Figure 9 shows the UV–vis absorption spectra of the CdTe/CdS QDs solubilized in toluene, after ligand exchange (information on the procedure can be found in the Supplementary Materials). The spectra revealed shifts similar to those observed for water-soluble CdTe/CdS QDs (Figure 7); that is, shifts toward longer wavelengths occurred in the spectra of the 1:1 and 1:2 systems, whereas the 1:4 and 1:8 presented shifts toward shorter wavelengths. The TEM micrograph (inset of Figure 9) shows that the nanocrystals' morphology did not change after growth of the CdS shell—the particles remained approximately spherical and well dispersed in organic solvent, with no aggregation on the carbon grid. The histogram of size distribution is showed in Figure S6. We achieved similar results for the other compositions.

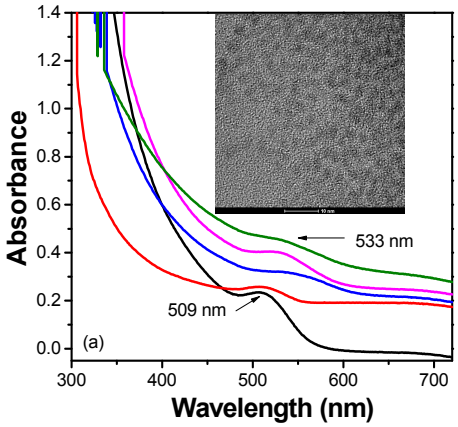

Figure 9. UV–vis absorption spectra of CdTe (black), CdTe/CdS core/shell growth with Cd^{2+}:thiourea (S^{2-}) molar ratios of 1:1, 1:2, 1:4, and 1:8 (red, blue, magenta, and olive lines, respectively). QDs containing DDT ligand were dispersed in toluene. Inset: TEM micrograph of CdTe/CdS 1:2.

Figure 10 contains the X-ray diffractograms of the CdTe nanocrystals and of the CdTe/CdS core/shell growth with Cd^{2+}:thiourea (S^{2-}) molar ratios of 1:1, 1:2, 1:4, and 1:8. The QDs displayed diffraction peaks at approximately 24.5°, 40.6°, and 48.0° (2θ), corresponding to the planes (111), (220), and (311), respectively, which refer to a crystalline structure of the zinc blende type [33]. The diffraction peaks shifted toward CdS as thicker CdS layers formed on the CdTe nanocrystals' surface. With the first addition of thiourea, a decrease in crystallinity was observed, and the diffraction peak shifted to the CdS crystalline planes. With the increase in ratio of Cd^{2+}:thiourea, there was no increase in crystallinity, indicating that the CdS shell did not grow considerably with increasing amounts of the precursor. This result corroborates the results of absorption, emission, and QY previously presented.

Figure S5 corresponds to the Fourier-transform infrared (FTIR) spectra of the CdTe/CdS growth with Cd^{2+}:thiourea (S^{2-}) molar ratios of 1:1, 1:2, 1:4, and 1:8. The bands centered at ~3400 cm^{-1} refer to the O–H bond stretching. The band located at 1635 cm^{-1} is assigned to bending in primary amines; this result indicates that possibly a part of the thiourea that was used as a source of sulfur can remain undegraded and remains acting as a surface ligand. The bands in the 1558 and 1429 cm^{-1} regions were associated with the COO^- group's asymmetric and symmetric stretchings, respectively. The bands in the regions 1350–1000 cm^{-1} and 700–600 cm^{-1} were attributed to the C–N, C–S, and C=S bond stretchings, respectively. The typical band of the S–H bond (2600–2550 cm^{-1}) was absent from the FTIR spectra of the core/shell systems, indicating that the MPA ligand remained bound to the QD surface by the end that originally contained the S–H group [26,37]. The spectra are similar in all samples, as expected.

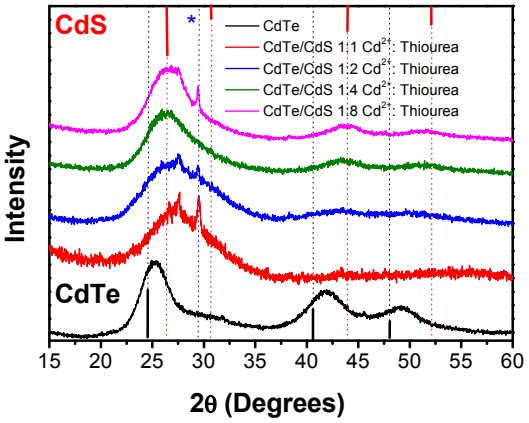

Figure 10. X-ray diffraction patterns of the CdTe and CdTe/CdS core/shell growth with Cd^{2+}:thiourea (S^{2-}) molar ratios of 1:1, 1:2, 1:4, and 1:8. * Impurities or byproducts not identified in the JCPDS database.

3. Discussions

In this work, we report the comparison of two methods of synthesis that are used in the literature for the synthesis of core/shell semiconductors, the SILAR method and the one-pot method. The SILAR method was studied with three CdTe cores of different sizes—2.17, 3.10, and 3.45 nm—and moreover, the thickness of the CdS shell was evaluated. It was observed that smaller cores are more susceptible to undergoing the compression effect of the CdS shell, and this effect is magnified with increasing thickness of the shell.

The compression effect causes a change in the core conduction-band level, shifting it to higher energy values and thus increasing the band gap of the material. The increased thickness of CdS semiconductor shell increases the size, and thus weakens the quantization, decreasing the band gap of the material. With these phenomena involved, the alignment of the core/shell that fell within the type I classification, which keeps all the charge carriers confined to the core, changes to the type II classification, in which the hole remains confined in the core (CdTe) and the electron confined in the shell (CdS). The type II configuration in the core/shell system tends to have lower QY values because

as the electron is confined in the shell, that is, on a surface region, it is more likely that the electron can be trapped in a surface trap, and finish by recombining nonradiatively. Thus, it was found that the photoluminescence QY decreased dramatically with increases of the shell on a small core, 2.17 nm. For larger QDs, 3.10 and 3.45 nm, due to their larger surface areas, but smaller area-to-volume ratios, the compression effect was not as pronounced as for the core of 2.17 nm, and, therefore the quantum efficiency was not decreased considerably.

Comparing the core/shell QDs prepared using the SILAR and one-pot methods, it was observed that the first method allows greater growth of CdS shell on the surface of the CdTe core, which can be observed by the larger displacement of the bands in the emission spectra, and by decrease in the oscillator strength of the absorption spectra (Figures 2a,b and 7a,b). While the SILAR method allowed preparing core/shell samples with maximum emission at 670 nm, the samples prepared using the one-pot method reached only 611 nm. This is due to the experimental conditions in each case. In the first, the sulfide precursor is a salt, sodium sulfide, so the anion diffuses and reacts rapidly on the surface of the crystal. Furthermore, the quantities of precursor are added successively, which enables a more controlled and homogeneous growth of the shell. In the one-pot method the precursor is molecular thiourea, which requires degradation of the molecule so that the sulfide is released. At low concentrations, with a maximum molar ratio of 2 (thiourea:Cd^{2+}), it was possible to grow the CdS shell by increasing the proportion of the precursor. However, in high molar ratios above 2, the precursor may cause steric hindrance and hinder the sulfide ions from reaching the surface of the nanocrystal, preventing the CdS shell from growing.

Regarding the homogeneity of material prepared using both methods, it can be said that the SILAR method allows more homogeneous growth of the CdS shell than the one-pot method. This assertion can be checked by comparing the diffractogram patterns of the samples prepared by the two methods, which demonstrates that the samples prepared using the SILAR method have greater crystallinity than those prepared using the one-pot method (Figures 3 and 10). A comparison between the methods reveals that although the SILAR method allows the growth of a more homogeneous and controlled shell, it is a time-consuming preparation method, and allowing further growth of CdS shell causes a compression effect on the small core of QDs. On the other hand, the one-pot method is simpler, and also allows high values of QY, even when used with small CdTe cores. Finally, to prepare a core/shell with excellent optical qualities and high photoluminescence QYs, in both methods of synthesis, it is desired to use a core of approximately 3.0 nm, and the shell grown on the surface should be not so thick, with two or three layers at maximum.

4. Materials and Methods

4.1. Reagents

Tellurium powder (200 mesh, 99.8%), 3-mercaptopropionic acid (MPA) (99%), Rhodamine 101 (100%), and 1-dodecanethiol (DDT, 98%) were obtained from Sigma-Aldrich (St. Louis, MO, USA). Sodium sulfide ($Na_2S{\cdot}9H_2O$, 98%) and thiourea (99%) were purchased from Synth (Diadema, São Paulo, Brazil). Sodium borohydride ($NaBH_4$, 97%) was acquired from Nuclear (São Paulo, Brazil). Cadmium chloride monohydrate ($CdCl_2{\cdot}H_2O$, 99%) was provided by Vetec (Rio de Janeiro, Brazil). All of the chemicals were used without additional purification. Ultrapure water (Millipore Co., Billerica, MA, USA) was employed in the synthesis of the nanoparticles.

4.2. CdTe Synthesis

The CdTe synthesis was performed according to reference [28]. To prepare a NaHTe solution, 0.8 mmol of Te powder and 1.6 mmol of $NaBH_4$ were mixed in 20 mL of ultrapure water, under an argon atmosphere. This solution was heated at 80 °C for 30 min. Next, 4 mL of the resulting NaHTe solution was transferred to another reaction vessel containing 0.4 mmol of $CdCl_2{\cdot}H_2O$ and 1.4 mmol of MPA dissolved in 80 mL of water; the pH of this solution had been previously adjusted to

10.0 by addition of NaOH (1 mol·L^{-1}). The molar ratio for Cd:Te:MPA was 1.0:0.4:3.5. This system was heated at 100 °C under an argon atmosphere at different synthesis times (10 min to obtain the core for the One-Pot procedure; 30 min, 3 h 30 min, and 6 h to obtain the CdTe cores for the SILAR experiments).

4.3. CdTe/CdS Synthesis Using the SILAR Method

The synthesis of the CdTe/CdS system using the SILAR technique was adapted from references [30,31]. It was conducted in two stages. Initially, it was necessary to prepare the CdTe nanocrystals; then, acetone (as a nonsolvent) was added to the solution containing the CdTe nanocrystals before shell growth, for purification purposes. After purification, the precipitate was dispersed in 20 mL of ultrapure water and heated at 40 °C under an argon atmosphere. CdS layers were deposited by successive injections of Cd and S ions solutions over the freshly prepared CdTe. The Cd precursor solution (0.03 mol·L^{-1}) was prepared by dissolving 0.6 mmol of $CdCl_2 \cdot H_2O$ and 1.4 mmol of MPA in 20 mL of water; the pH was adjusted to 10 by addition of NaOH (1 mol·L^{-1}). The sulfur precursor solution was obtained by dissolving 0.5 mmol of $Na_2S \cdot 9H_2O$ in 20 mL of water. Both solutions were prepared at room temperature, under an argon atmosphere. Next, the growth process was initiated; one to five CdS layers were grown over the CdTe core by successively injecting the cationic and anionic precursors over the solution containing the CdTe nanocrystals, at 0.1 mL·min^{-1}. Ten minutes were allowed to elapse between each addition. To determine the amount of Cd and S required for each monolayer, it was necessary to know the number of surface atoms present in a given core/shell system [25]. This information was obtained by calculating the nanocrystals' concentration, as estimated using the Beer-Lambert law. Using this information and also knowing the nanocrystals and CdTe mean sizes, it was possible to determine the molar quantity of precursors that was required to grow each layer [30]. To verify the effect of core size on the QDs' optical properties, CdTe nanocrystals of different sizes (CdTe nanocrystals of 2.17 nm, 3.10 nm, and 3.45 nm, obtained after 30 min, 3 h 30 min, and 6 h of synthesis, respectively) were coated with CdS layers of different thickness using the same experimental procedure described above.

4.4. CdTe/CdS Synthesis by the One-Pot Approach

The procedure to obtain the CdTe/CdS was adapted from references [29,32,36]. After the solution containing the CdTe nanocrystals was prepared, 0.3 mmol of thiourea, used as the sulfur precursor, was added to the freshly nonpurified CdTe solution; this amount of thiourea provided a Cd:S stoichiometric ratio of 1:1. The final solution was submitted to 4-h controlled stirring and heating under an argon atmosphere. Some aliquots were withdrawn from the reaction medium at regular time intervals; their absorption and emission spectra were recorded, to monitor the synthesis. At the end of the reaction, acetone was added, and after centrifugation the QDs were obtained as a powder. This stage was repeated several times, to purify the QDs. To increase the CdS shell thickness, the same synthetic procedure was conducted, but the Cd:S stoichiometric ratios were increased to 1:2, 1:4, and 1:8, by increasing the amount of thiourea that was added to the reaction.

4.5. Characterization

UV–vis absorption and PL spectra were acquired on a Varian Cary 50 spectrophotometer (Varian Inc., Palo Alto, CA, USA) and Shimadzu RF-5301 PC spectrofluorophotometer (Shimadzu Corporation, Nakagyo-ku, Kyoto, Japan), respectively. The spectrofluorophotometer was equipped with a 150-W xenon lamp. The absorption and fluorescence measurements were typically performed with 10-mm quartz cuvettes (Shimadzu) using air-saturated solutions at room temperature. The fluorescence QY of the QDs was estimated using the comparative method of Williams et al. [34] considering some current recommendations [38,39]. Powder X-ray diffraction (XRD) patterns were recorded on a Shimadzu XRD-6000 apparatus using CuKα radiation. FTIR spectra of the materials were obtained by the conventional KBr pellet technique, on a GXI spectrum Perkin Elmer spectrometer (PerkinElmer, Waltham, MA, USA), operating between 4000 and 400 cm^{-1}. At least 32 scans were

registered, with a resolution of 2 cm^{-1}. Transmission electron microscopy (TEM) was performed on a Tecnai-G2-20-FEI microscope operating at 200 kV. Liquid samples were dispersed onto carbon-coated 400-mesh copper grids. To avoid aggregation of the QDs on the grids, the surface ligand was changed from MPA to DDT, with the samples dispersed in toluene. The images were processed using the ImageJ software.

5. Conclusions

We successfully synthesized CdTe/CdS core/shell systems via the SILAR and one-pot approaches; we used MPA as ligand in both cases. The absorption bands of the materials obtained using the one-pot strategy shifted to lower wavelength as the CdS shell thickness increased.

The SILAR method allowed us better to control the optical properties of the prepared CdTe/CdS QDs. The deposition of thicker CdS layers (three to five layers) on smaller CdTe nanocrystals surface (CdTe nanocrystals of 2.17 nm) possibly evoked transformation of the core/shell type I system into type II, as demonstrated by the less intense absorption and emission bands. Larger nanocrystals (CdTe nanocrystals of 3.10 nm and CdTe nanocrystals of 3.45 nm) did not display this behavior because they were less susceptible to strain effects. This also accounted for the larger absorption and emission band displacements obtained in the case of CdTe nanocrystals of 2.17 nm. The latter nanocrystals also afforded QDs with lower QYs. The larger CdTe nanocrystals coated with three CdS layers provided maximum photoluminescence QY.

While the SILAR method produces a better control in the growing of the CdS shell, giving rise to higher fluorescence quantum yield values, the one-pot method allows the obtention of nanoparticles with moderate fluorescence quantum yield, but it is faster from the experimental point of view. Both methods were shown to be reproducible in the experimental conditions described here. Therefore, the choice of the method to synthesize CdTe/CdS core/shell nanoparticles depends on the experimental conditions or the desired optical properties.

Supplementary Materials: The following are available online at http://www.mdpi.com/2073-4352/6/10/133/s1, How to determine the amount of precursors of Cd^{2+} and S^{2-} to grow a core/shell; Tables S1–S3: Molar quantities of the Cd and S precursors necessary to grow between one and five CdS layers around CdTe nanocrystals of different sizes; Figure S1: Histogram of the particle size distribution of CdTe obtained with 4 h of synthesis. Figures S2 and S3: UV–vis absorption (a), PL (b), and (c) spectra of CdTe/CdS QDs prepared with one to five layers of CdS, and CdTe nanocrystals with different sizes; Determination of the Fluorescence Quantum Yield (QY); Figure S4: Relationship between absorbance and integrated fluorescence intensity for Rhodamine 101 (standard) and CdTe/CdS QDs with three CdS layers. Figure S5: FTIR spectra of the CdTe/CdS core/shell growth with Cd^{2+}:thiourea (S^{2-}) molar ratios of 1:1, 1:2, 1:4, and 1:8. Figure S6: Histogram of the particle size distribution of CdTe/CdS 1:2 obtained.

Acknowledgments: This work was supported by CAPES, FINEP, CNPq, and FAPEMIG. The authors would like to acknowledge the Center of Microscopy at UFMG (http://www.microscopia.ufmg.br) for providing the equipment and technical support for the experiments involving TEM. We also thank Peter Reiss (CEA-Grenoble-France) for helpful discussions.

Author Contributions: Marco A. Schiavon and Fernanda O. Silva conceived and designed the experiments; Brener R. C. Vale, Fernanda O. Silva, Melissa S. Carvalho, and Ellen Raphael performed the experiments; Brener R. C. Vale, Fernanda O. Silva, Ellen Raphael, and Marco A. Schiavon analyzed the data; Brener R. C. Vale, Marco A. Schiavon and Jefferson L. Ferrari wrote the paper.

Conflicts of Interest: The authors declare no conflicts of interest. The founding sponsors had no role in the design of the study; in the collection, analyses, or interpretation of data; in the writing of the manuscript, and in the decision to publish the results.

References

1. Hetsch, F.; Xu, X.; Wang, H.; Kershaw, S.V.; Rogach, A.L. Semiconductor nanocrystal quantum dots as solar cell components and photosensitizers: Material, charge transfer, and separation aspects of some device topologies. *J. Phys. Chem. Lett.* **2011**, *2*, 1879–1887. [CrossRef]
2. Kamat, P.V. Quantum dot solar cells. The next big thing in photovoltaics. *J. Phys. Chem. Lett.* **2013**, *4*, 908–918. [CrossRef] [PubMed]

3. Ruhle, S.; Shalom, M.; Zaban, A. Quantum-dot-sensitized solar cells. *ChemPhysChem* **2010**, *11*, 2290–2304. [CrossRef] [PubMed]
4. Konstantatos, G.; Sargent, E.H. *Colloidal Quantum Dots Optoelectronics and Photovoltaics*; Cambridge University Press: Cambridge, UK, 2013.
5. Alivisatos, A.P.; Gu, W.; Larabell, C. Quantum dots as cellular probes. *Ann. Rev. Biomed. Eng.* **2005**, *7*, 55–76. [CrossRef] [PubMed]
6. Manzoor, K.; Johny, S.; Thomas, D.; Setua, S.; Menon, D.; Nair, S. Bio-conjugated luminescent quantum dots of doped ZnS: A cyto-friendly system for targeted cancer imaging. *Nanotechnology* **2009**, *20*, 065102. [CrossRef] [PubMed]
7. Silva, F.O.; Viol, L.C.d.S.; Ferreira, D.L.; Alves, J.L.A.; Schiavon, M.A. Estado da arte da síntese de semicondutores. *Quím. Nova* **2010**, *33*, 1933–1939. [CrossRef]
8. Fontes, A.; Santos, B.S. *Quantum Dots: Applications in Biology*, 2nd ed.; Humana Press: New York, NY, USA, 2014; Volume 1, p. XI 258.
9. Chatterjee, K.; Sarkar, S.; Rao, K.J.; Paria, S. Core/shell nanoparticles in biomedical applications. *Adv. Colloid Interface Sci.* **2014**, *209*, 8–39. [CrossRef] [PubMed]
10. Zhang, H.; Cui, Z.; Wang, Y.; Zhang, K.; Ji, X.; Lü, C.; Yang, B.; Gao, M. From water-soluble CdTe nanocrystals to fluorescent nanocrystal-polymer transparent composites using polymerizable surfactants. *Adv. Mater.* **2003**, *15*, 777–780. [CrossRef]
11. Talapin, D.V.; Poznyak, S.K.; Gaponik, N.P.; Rogach, A.L.; Eychmüller, A. Synthesis of surface-modified colloidal semiconductor nanocrystals and study of photoinduced charge separation and transport in nanocrystal-polymer composites. *Physica E* **2002**, *14*, 237–241. [CrossRef]
12. Rogach, A.L. *Semiconductor Nanocrystal Quantum Dots*; Rogach, A.L., Ed.; Springer: Wien, Austria, 2008.
13. Aldeek, F.; Balan, L.; Medjahdi, G.; Roques-Carnes, T.; Malval, J.-P.; Mustin, C.; Ghanbaja, J.; Schneider, R. Enhanced optical properties of core/shell/shell CdTe/CdS/ZnO quantum dots prepared in aqueous solution. *J. Phys. Chem. C* **2009**, *113*, 19458–19467. [CrossRef]
14. Peng, H.; Zhang, L.; Soeller, C.; Travas-Sejdic, J. Preparation of water-soluble CdTe/CdS core/shell quantum dots with enhanced photostability. *J. Lumin.* **2007**, *127*, 721–726. [CrossRef]
15. Chaudhuri, R.G.; Paria, S. Core/shell nanoparticles: Classes, properties, synthesis mechanisms, characterization, and applications. *Chem. Rev.* **2012**, *112*, 2373–2433. [CrossRef] [PubMed]
16. Ivanov, S.A.; Piryatinski, A.; Nanda, J.; Treitak, S.; Zavadil, K.R.; Wallace, W.O.; Werder, D.; Klimov, V.I. Type-II core/shell CdS/Zn Senanocrystals: Synthesis, electronic structures, and spectroscopic properties. *J. Am. Chem. Soc.* **2007**, *129*, 11708–11719. [CrossRef] [PubMed]
17. Kim, S.; Fisher, B.; Eisler, H.-J.; Bawendi, M. Type-II quantum dots: CdTe/CdSe (core/shell) and CdSe/ZnTe (core/shell) heterostructures. *J. Am. Chem. Soc.* **2003**, *125*, 11466–11467. [CrossRef] [PubMed]
18. Smith, A.M.; Mohs, A.M.; Nie, S. Tuning the optical and electronic properties of colloidal nanocrystals by lattice strain. *Nat. Nanotechnol.* **2008**, *4*, 56–63. [CrossRef] [PubMed]
19. Liu, Y.-F.; Yu, J.-S. Selective synthesis of CdTe and high luminescence CdTe/CdS quantum dots: The effect of ligands. *J. Colloid Interfaces Sci.* **2009**, *333*, 690–698. [CrossRef] [PubMed]
20. Ivanov, S.A.; Nanda, J.; Piryatinski, A.; Achermann, M.; Balet, L.P.; Bezel, I.V.; Anikeeva, P.O.; Tretiak, S.; Klimov, V.I. Light amplification using inverted core/shell nanocrystals: Towards lasing in the single-exciton regime. *J. Phys. Chem. B* **2004**, *108*, 10625–10630. [CrossRef]
21. Shi, A.; Sun, J.; Zeng, Q.; Shao, C.; Sun, Z.; Li, H.; Kong, X.; Zhao, J. Photoluminescence quenching of CdTe/CdS core-shell quantum dots in aqueous solution by ZnO nanocrystals. *J. Lumin.* **2011**, *131*, 1536–1540. [CrossRef]
22. Kuo, K.-T.; Liu, D.-M.; Chen, S.-Y.; Lin, C.-C. Core-shell $CuInS_2$/ZnSquantum dots assembled on short ZnOnanowires with enhanced photo-conversion efficiency. *J. Mater. Chem.* **2009**, *19*, 6780–6788. [CrossRef]
23. Kim, M.R.; Ma, D. Quantum-dot-based solar cells: Recent advances, strategies, and challenges. *J. Phys. Chem. Lett.* **2015**, *6*, 85–99. [CrossRef] [PubMed]
24. Gu, Z.; Zou, L.; Fang, Z.; Zhu, W.; Zhong, X. One-pot synthesis of highly luminescent CdTe/CdS core/shell nanocrystals in aqueous phase. *Nanotechnology* **2008**, *19*, 135604–135611. [CrossRef] [PubMed]
25. Li, J.J.; Wang, Y.A.; Guo, W.; Keay, J.C.; Mishima, T.D.; Johnson, M.B.; Peng, X. Large-scale synthesis of nearly monodisperse CdSe/CdS core/shell nanocrystals using air-stable reagents via successive ion layer adsorption and reaction. *J. Am. Chem. Soc.* **2003**, *125*, 12567–12575. [CrossRef] [PubMed]

26. Zeng, Q.; Kong, X.; Sun, Y.; Zhang, Y.; Tu, L.; Zhao, J.; Zhang, H. Synthesis and optical properties of type II CdTe/CdS core/shell quantum dots in aqueous solution via successive ion layer adsorption and reaction. *J. Phys. Chem. C* **2008**, *112*, 8587–8593. [CrossRef]
27. Van Embden, J.; Jasieniak, J.; Gómes, D.E.; Mulvaney, P.; Giersig, M. Review of the synthetic chemistry involved in the production of core/shell semiconductor nanocrystals. *Aust. J. Chem.* **2007**, *60*, 457–471. [CrossRef]
28. Silva, F.O.; Carvalho, M.S.; Mendonça, R.; Macedo, W.A.A.; Balzuweit, K.; Reiss, P.; Schiavon, M.A. Effect of surface ligands on the optical properties of aqueous soluble CdTe quantum dots. *Nanoscale Res. Lett.* **2012**, *7*, 536. [CrossRef] [PubMed]
29. Yu, W.W.; Qu, L.; Guo, W.; Peng, X. Experimental determination of the extinction coefficient of CdTe, CdSe, and CdS nanocrystals. *Chem. Mater.* **2003**, *15*, 2854–2860. [CrossRef]
30. Reiss, P.; Protière, M.; Li, L. Core/shell semiconductor nanocrystals. *Small* **2009**, *5*, 154–168. [CrossRef] [PubMed]
31. Dorfs, D.; Franzl, T.; Osovsky, R.; Brumer, M.; Lifshitz, E.; Klar, T.A.; Eychmüller, A. Type I and type II nanoscale heterostructures based on CdTe nanocrystals: A comparative study. *Small* **2008**, *4*, 1148–1152. [CrossRef] [PubMed]
32. Wang, L.; Wang, H.-Y.; Gao, B.-R.; Pan, L.-Y.; Jiang, Y.; Chen, Q.-D.; Han, W.; Sun, H.-B. Transient absorption spectroscopic study on band-structure-type change in CdTe/CdS core-shell quantum dots. *IEEE J. Quantum Electron.* **2011**, *47*, 1177–1184. [CrossRef]
33. Rogach, A.L. Nanocrystalline CdTe and CdTe(s) particles: Wet chemical preparation, size-dependent optical properties and perspective of optoelectronic applications. *Mater. Sci. Eng. B* **2000**, *69*, 435–440. [CrossRef]
34. Williams, A.T.R.; Winfield, S.A.; Miller, J.N. Relative fluorescence quantum yield using a computer-controlled luminescence. *Analyst* **1983**, *108*, 1067–1071. [CrossRef]
35. Chen, C.-Y.; Cheng, C.-T.; Yu, J.-K.; Pu, S.-C.; Cheng, Y.-M.; Chou, P.-T. Spectroscopy and femtosecond dynamics of type-IICdSe/ZnTe core-shell semiconductor synthesized via the CdO precursor. *J. Phys. Chem. B* **2004**, *108*, 10687–10691. [CrossRef]
36. Gui, R.; An, X.; Su, H.; Shen, W.; Chen, Z.; Wang, X. A near-infrared-emitting CdTe/CdS core/shell quantum dots-based off-on fluorescence sensor for highly selective and sensitive detection of Cd^{2+}. *Talanta* **2012**, *94*, 257–262. [CrossRef] [PubMed]
37. Vale, B.R.C.; Vieira, K.O.; Sousa, J.C.L.; Ferrari, J.L.; Schiavon, M.A. Efeito da estrutura molecular de ligantes de superfícies em pontos quânticos de CdTe dispersos em água. *Quím. Nova* **2015**, *38*, 22–29.
38. Resch-Genger, U.; Rurack, K. Determination of the photoluminescence quantum yield of dilute dye solutions (IUPAC technical report). *Pure Appl. Chem.* **2013**, *85*, 2005–2026. [CrossRef]
39. Brouwer, A.M. Standards for photoluminescence quantum yield measurements in solution (IUPAC technical report). *Pure Appl. Chem.* **2011**, *83*, 2213–2228. [CrossRef]